zFP538, a Yellow-Fluorescent Protein from *Zoanthus*, Contains a Novel Three-Ring Chromophore[†,‡]

S. James Remington,[*,§] Rebekka M. Wachter,[§,||] Daniel K. Yarbrough,[§] Bruce Branchaud,[§] D. C. Anderson,[§] Karen Kallio,[§] and Konstantin A. Lukyanov[⊥]

Institute of Molecular Biology, Departments of Physics, Chemistry, and Biology, University of Oregon, Eugene, Oregon 97403-1229, and Shemiakin and Ovchinnikov Institute of Bioorganic Chemistry, Russian Academy of Sciences, Miklukho-Maklaya 16/10, 117997 Moscow, Russia

Received July 28, 2004; Revised Manuscript Received October 15, 2004

ABSTRACT: Crystal structures of the tetrameric yellow-fluorescent protein zFP538 from the button polyp *Zoanthus* sp. and a green-emitting mutant (K66M) are presented. The atomic models have been refined at 2.7 and 2.5 Å resolution, with final crystallographic *R* factors of 0.206 (R_{free} = 0.255) and 0.190 (R_{free} = 0.295), respectively, and have excellent stereochemistry. The fold of the protomer is very similar to that of green (GFP) and red (DsRed) fluorescent proteins; however, evidence from crystallography and mass spectrometry suggests that zFP538 contains a three-ring chromophore derived from that of GFP. The yellow-emitting species (λ_{em}^{max} = 538 nm) is proposed to result from a transimination reaction in which a transiently appearing DsRed-like acylimine is attacked by the terminal amino group of lysine 66 to form a new six-membered ring, cleaving the polypeptide backbone at the 65−66 position. This extends the chromophore conjugation by an additional double bond compared to GFP, lowering the absorption and emission frequencies. Substitution of lysine 66 with aspartate or glutamate partially converts zFP538 into a red-fluorescent protein, providing additional support for an acylimine intermediate. The diverse and unexpected roles of the side chain at position 66 give new insight into the chemistry of chromophore maturation in the extended family of GFP-like proteins.

The remarkable diversity of coral reef coloration is in a large part due to the presence of fluorescent proteins (*1*) and nonfluorescent chromoproteins (*2*−*4*) that are distantly related to the green-fluorescent protein (GFP)[1] from *Aequorea victoria*. The light absorption and emission characteristics of these molecules span most of the visible spectrum, yet they can generally be grouped into four major emission classes, suggesting that the light-emitting species are chemically distinct yet few in types (*5*−*7*). From emission properties, these groupings generally comprise fluorescent proteins with cyan, green (GFP-like), yellow, and red emission, as well as nonfluorescent chromoproteins with appearance ranging from blue to purple in color. The red-emitting proteins and nonfluorescent chromoproteins are closely related in amino acid sequence and their respective emission properties can be interconverted by a small number of point mutations (*8*−*10*).

The reef fluorescent proteins have considerable potential for biotechnology, for example, in multicolor labeling and resonance energy-transfer applications (*7*). However, the naturally occurring variants suffer from serious disadvantages such as their oligomeric composition and slow and incomplete maturation. In one approach to solve these problems, Campbell et al. expended considerable effort to produce a monomeric red-fluorescent protein from the tetrameric DsRed (*11*). As an alternative, one could rationally modify monomeric GFP to produce a wider range of emission colors. Despite recent advances in our understanding of the mechanism of GFP chromophore formation (*12*, *13*), the latter approach will require a much more thorough comprehension of the maturation process than is presently the case. For the reef chromoproteins, even the precise nature of the chromophore remains in most cases to be established.

In DsRed, a multistep process first produces a GFP-like intermediate that is further oxidized to an acylimine [(*14*−*17*), see Figure 1a]. In the final step, the chromophore conjugation is extended through the polypeptide backbone, which adequately accounts for the red-shifted absorption and emission spectra (*15*) compared to GFP. High-resolution three-dimensional structures of DsRed (*18*, *19*) confirmed the nature of the red-emitting chromophore, but the catalytic steps leading to acylimine formation remain unclear. There is good evidence that a DsRed-like acylimine linkage is present in other fluorescent proteins (e.g., eqFP611) (*20*),

[†] This work was supported by NSF MCB-0111053 (to S.J.R.), NIH predoctoral traineeship (GM-00759) (to D.K.Y.), a grant for Molecular and Cellular Biology from the Russian Academy of Sciences (to K.L.), and NIH postdoctoral fellowship 1F32GM19075 (to R.M.W.).

[‡] Coordinates and structure factors have been deposited in the Protein Data Bank, access codes 1XAE (wild type) and 1XA9 (K66M).

[*] To whom correspondence should be addressed. E-mail: jremington@uoxray.uoregon.edu. Telephone: (541) 346-5190. Fax: (541) 346-5870.

[§] University of Oregon.

[||] Present address: Department of Chemistry, Arizona State University, Tempe, AZ 85287.

[⊥] Russian Academy of Sciences.

[1] Abbreviations: drFP583 (DsRed), *Discosoma* sp. red-fluorescent protein; zFP538, *Zoanthus* sp. yellow-fluorescent protein; GFP, *Aequorea victoria* green-fluorescent protein; FRET, fluorescence resonance energy transfer; SDS−PAGE, sodium dodecyl sulfate−polyacrylamide gel electrophoresis; HPLC, high-performance liquid chromatography; MS, mass spectrometry; rms, root mean square.

10.1021/bi048383r CCC: $30.25
Published on Web 12/03/2004

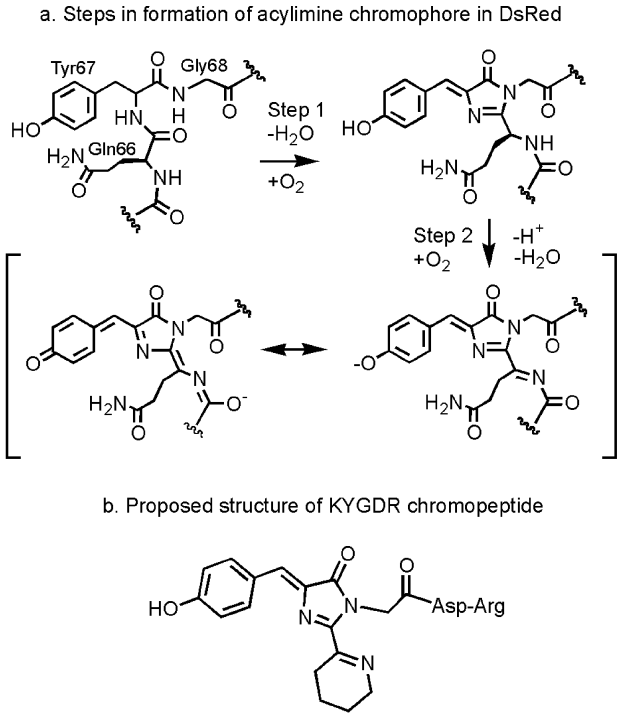

FIGURE 1: (a) Steps outlining proposed chromophore formation in DsRed assuming a neutral GFP-like intermediate, adapted from refs *15*, *16*, and *18*. (b) Proposed structure of chromophore in wild-type zFP538.

as well as in the nonfluorescent chromoproteins Rtms5 (*21*) and gtCP (*22*). The acylimine linkage is reactive, and when subjected to harsh conditions, the polypeptide backbone is hydrolyzed (*15*, *22*). Thus, in other GFP-like proteins, the acylimine could serve as an intermediate for further steps in the maturation process.

The yellow-fluorescent protein (zFP538, $\lambda_{em}^{max} = 538$ nm) isolated from the button polyp *Zoanthus* (*1*) is an interesting case because the emission maximum is approximately centered between those of GFP (508 nm) and DsRed (583 nm). The amino acid sequence comprising the mature chromophore of zFP538 is -Lys66-Tyr67-Gly68- (for sequence alignments, see Supplementary Table 1 in the Supporting Information). Gurskaya et al. (*23*) investigated factors that determine the emission color of zFP538 and concluded that Lys 66 is critical for yellow emission. More recently, Zagranichny et al. (*24*) described the behavior of zFP538 under mildly denaturing conditions and subjected several proteolytically derived chromopeptides to extensive analysis. They concluded that the polypeptide backbone was likely fragmented at the 65−66 position within the intact protein and that the chromophore contains an imino group at the Lys 66 Cα that is responsible for the red shift of zFP538 compared to GFP. The analysis is complicated, however, by reactions that the isolated chromopeptide may undergo in aqueous solution, especially at extreme pH values.

Here, we establish that yellow emission in zFP538 arises from a novel three-ring chromophore in which the side chain of Lys 66 cyclizes (Figure 1b) to form the third ring. The cyclization reaction evidently results in cleavage of the main chain within the folded protein. We propose that the ring forms upon nucleophilic attack by the lysine Nϵ upon a transient acylimine intermediate formed from the peptide bond between residues 65 and 66. The conjugation in the chromophore thus formed is intermediate to those of GFP and DsRed, accounting for the yellow appearance of the emission. The mechanistic role played by position 66 of the chromophore triplet is unexpected but may be a rather general phenomenon in the family of GFP-like proteins.

MATERIALS AND METHODS

Mutagenesis and Protein Expression. Expression vectors in the pQE-30 (Qiagen, Chatsworth, CA) expression system for wild-type zFP538 and K66M zFP538 containing an N-terminal $(His)_6$ purification tag were generously provided by Clontech, Inc. (Palo Alto, CA).

All possible variants of zFP538 at position 66 were generated by PCR-based site-directed mutagenesis (QuikChange, Stratagene) using the primers

5′-gacatattgtcagctggctttnnntacggagacaggattttcactg-3′

5′-cagtgaaaatcctgtctccgtannnaaagccagctgacaatatgtc-3′

where n is any nucleotide. PCR was carried out, and products were transformed into *Escherichia coli* JM-109(DE3) cells. Approximately 10 colonies per PCR reaction were sequenced. Five PCR reactions were sufficient to generate 16 mutants, and specific primers were used to generate the remaining three by conventional site-directed mutagenesis. After sequence verification, mutant plasmids were transformed into fresh JM-109(DE3) cells and cells were plated onto 150 mm Petri plates for protein expression. Expression plates consisted of a bottom layer of ∼40 mL of LB agar (7.5 g/L) with 90 μg/mL carbenicillin and 1% lactose (to provide induction) and a top layer of LB agar (15 g/L) with 90 μg/mL carbenicillin.

Protein was produced by one of two procedures, either from 4 L cultures of *E. coli* strain JM-109 with an induction period of 6 h and purified over Ni-NTA agarose (Qiagen) as previously described (*18*) or by streaking out 200 μL of a 5 mL overnight culture grown in LB plus ampicillin onto five 150 × 15 mm plates containing LB agar plus 1% lactose and 50 μg/mL carbenicillin. The plates were kept in at 37 °C for 48 h and then transferred to room temperature for another 24 h. The yellowish orange lawn of bacteria was scraped off the plates, and cells were suspended in 50 mM HEPES, 0.3 M NaCl, 10% glycerol, and 2 mM BME with 0.1 mM PMSF and disrupted by sonication. Purified protein was dialyzed into 50 mM HEPES at pH 7.9, 0.3 M NaCl, and 1 mM β-mercaptoethanol and concentrated by ultrafiltration.

Fluorescence Maturation Assay. For quantitative time-course observations of protein maturation, 100 mL cultures were induced with IPTG for 2 h and then immediately harvested by centrifugation and the pellets were frozen at −20 °C overnight. Pellets were resuspended in 2.0 mL of lysis buffer (50 mM HEPES at pH 7.9, 300 mM NaCl, and 10% glycerol) and lysed for 20 min on ice with lysozyme (Sigma) and DNAse 1 (Roche). Lysates were cleared by centrifugation for 10 min, and the protein was purified using a Ni-NTA agarose column (Qiagen). PD-10 sepharose columns (Pharmacia) were used to exchange samples into 50 mM HEPES at pH 7.9, 300 mM NaCl, and 100 mM imidazole buffer, with the final protein concentration varying between 0.2 and 0.5 mg/mL. Time-dependent absorbance

and fluorescence measurements were carried out at 15 °C using a Shimadzu UV-2101PC spectrophotometer and a Perkin−Elmer LS-55 fluorometer. Scans were collected 0.5 h after the onset of purification and thereafter every hour for 60−100 h. Emission intensity was scanned from 400 to 700 nm (λ_{ex} = 280 nm).

Gel Analysis. Sodium dodecyl sulfate−polyacrylamide gel electrophoresis (SDS−PAGE) gel analysis was carried out on zFP538 and DsRed to compare fragmentation behavior as a function of boiling time (0−24 min) and as a function of acid or base denaturation. The acid-denaturation protocol involved adding 1 μL of 10 M HCl to 10 μL of protein solution followed by immediate addition of 10 μL of 2× SDS sample buffer. The sample was then neutralized by immediate addition of 9 μL of 1.0 M NaOH and loaded onto the gel. In the base-denaturation protocol, the addition of NaOH and HCl was reversed, with identical concentrations and quantities.

Mass Spectrometry (MS). Peptides containing the chromophore were isolated by the following procedure. Purified, His-tagged zFP538 at 5 mg/mL was combined in a 1:2 ratio with 8 M urea in 50 mM HEPES at pH 7.9, 0.3 M NaCl, and 20 mM methylamine and heated to 106 °C for 2.5 min. The denatured protein was reapplied to a Ni-NTA column, and the flow-through was diluted to a final urea concentration of 1.7 M. The protein was concentrated to 0.8 mg/mL by ultrafiltration (Centricon). Trypsin was then added in a 1:20 (w/w) ratio, and the digest was carried out at 37 °C for 24 h. The chromopeptide was isolated by high-performance liquid chromatography (HPLC) on a Vydac C18 column, 2.1 × 250 mm, with a 0−100% acetonitrile gradient in 0.1% trifluoroacetic acid. Two peptide peaks with absorbance at 380 nm were collected and analyzed by MS. The chromopeptide was diluted 1:10 (v/v) in matrix solution consisting of 0.5 mg/mL of α-cyano-4-hydroxycinnamic acid (Sigma−Aldrich Chemical Co., St. Louis, MO) dissolved in 50% acetone−water. A total of 1 μL was spotted on a sample plate and examined by MALDI−ion trap MS using a Masstech (Burtonsville, MD) atmospheric pressure−MALDI source and a ThermoFinnigan (San Jose, CA) LCQ Deca XP Plus mass spectrometer operating with an ion-transfer capillary temperature of 350 °C and maximum ion inject time of 500 ms. Samples of the matrix alone were run as the controls in all of the experiments.

Crystal Growth and Data Collection. Hexagonal crystals of K66M zFP538 were grown by vapor diffusion in 4−8 μL of hanging drops containing equal volumes of protein solution (A_{280} = 47 in 50 mM HEPES at pH 7.9 and 300 mM NaCl) and reservoir solution (2 M ammonium sulfate, 25−30% ethylene glycol, and 100 mM PIPES at pH 6.5). The crystals grew at room temperature over a period of 1 month and were typically 0.2 × 0.3 × 0.4 mm. Diffraction data were collected from a single flash-frozen crystal at 100 K at the Stanford Synchrotron Radiation Laboratory, beam line 7-1, at a wavelength of 1.08 Å on a Mar345 image plate. The diffraction data were integrated using MOSFLM (*25*) and scaled and merged to 2.5 Å resolution using SCALA (*26*).

Crystals of wild-type zFP538 were obtained using hanging-drop vapor diffusion with 4 μL drops of protein (A_{280} = 17 in standard buffer) added to 4 μL of a well solution (50 mM CHES at pH 9.0 and 1.8 M $AmSO_4$) plus 1 μL of β-mercaptoethanol (required) per 1 mL of well solution. Crystals were extremely difficult to obtain, with only two useful examples appearing after 6−18 months at 15 °C. For data collection, a single crystal (∼0.4 mm in each dimension) was passed quickly through a drop of 1.7 M AmSO4, 50 mM CHES at pH 9.0, and 25% glycerol and flash frozen at 100 K. Data were collected using an R-axis IV (Molecular Structure Corporation) image plate detector on a conventional generator. Images were indexed and processed with the HKL suite (*27*).

Structure Solution, Model Building, and Refinement. K66M zFP538 crystallized in spacegroup $P6_222$ with cell dimensions a = 108.4 and c = 84.9 Å, with one molecule per asymmetric unit (packing coefficient V_m = 2.7 Å^3/Da). The protomer is adjacent to a position with 222 point symmetry, forming the expected tetramer. The structure of K66M zFP538 was solved via molecular replacement with EPMR (*28*) using the DsRed A chain (PDB ID code 1G7K) (*18*) as a search model. Rigid-body refinement was performed using TNT (*29*), followed by model building with O (*30*). The electron density map permitted modeling of residues 4−230. Cys 87 was modeled with a disulfide linkage to a molecule of β-mercaptoethanol as suggested by strong electron density peaks adjacent to the sulfur atom. Several other cysteines appeared to be oxidized and were modeled as cysteic acid. Positional and *B*-factor refinements were performed using CNS (*31*) and TNT for all data (no σ or F cutoffs) in the resolution range of 6.0 Å or higher. Water molecules were modeled into strong difference density peaks that were within hydrogen-bonding distance to appropriate partners. The free *R* factor was estimated from 10% of the data after simulated annealing against 90% of the data using CNS and/or TNT to eliminate model memory from the test set (estimate of free *R a posteriori*) (*32*).

Crystals of wild-type zFP538 were obtained in space group $P3_121$, with a = 121.16 Å and c = 111.69 Å. The diffraction data are weak and of rather low quality as judged from merging *R* factors, which may be attributed to loose packing (V_m = 4.2 Å^3/Da), protein oxidation, and other processes taking place during the extended crystal growth period (up to 1.5 years). However, the 8-fold redundancy of data collection helped to produce a usable data set. There are two protomers (an A−B dimer) in the asymmetric unit. The structure was solved by molecular replacement with the refined K66M model and refined using the procedures outlined above. In the early stages, electron density maps were averaged about the local 2-fold axis and the model was refined using strict NCS restraints. The chromophore was not modeled into the electron density maps until the crystallographic *R* factor was lowered to about 0.25 for 2.7 Å data using tight NCS restraints. At this point, ($F_o - F_c$) and ($2F_o - F_c$) omit electron density maps (Figure 2) were very similar for the two independent monomers in the asymmetric unit, and each clearly revealed the internal chain break. The maps could be readily interpreted in terms of the novel structure; therefore, the NCS restraints were removed and the model was refined to convergence.

RESULTS AND DISCUSSION

Atomic Models. Crystallographic analyses of wild-type zFP538 and a green mutant K66M have been performed at

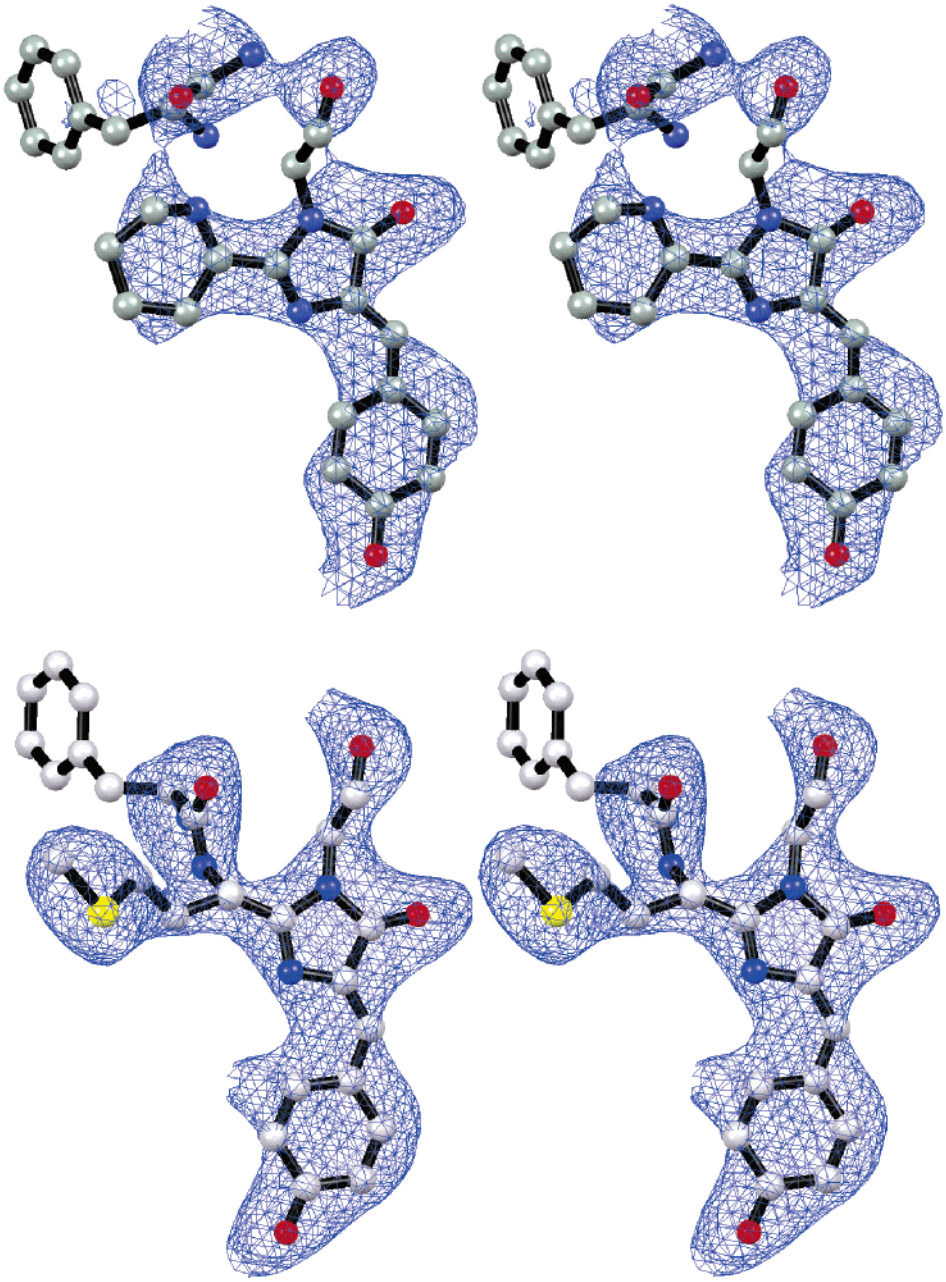

FIGURE 2: Portions of $F_o - F_c$ omit electron density maps contoured at 2.0σ for wild-type zFP538, molecule A (top), and the green mutant K66M zFP538 (bottom). Phases were calculated after omission of the chromophore and the atoms associated with the Phe 65 backbone linkage, followed by 20 cycles of crystallographic refinement. The ring of Phe 65 was included in the phase calculation as a control. The final refined atomic models are superimposed in ball-and-stick representation with oxygen, red; nitrogen, blue; and sulfur, yellow.

nominal resolutions of 2.7 and 2.5 Å, respectively, in two different crystal forms. The final crystallographic statistics (Table 1) are satisfactory, and the models have excellent stereochemistry. PROCHECK (*33*) reports overall *G* values per monomer to be in the range of −0.02 to 0.01. There are no residues in either the disallowed or "generously allowed" regions of the Ramachandran diagram. However, only weak electron density is present for residues 210−213, indicating disorder; therefore, coordinates for these atoms must be regarded as unreliable.

In each crystal, the protomer forms a close-packed tetramer similar to DsRed (*18*, *19*). The three monomers in the asymmetric units of the two crystal forms are identical within the error of the structure determination [root-mean-square (rms) deviation ~0.36 Å for α-carbon superposition], except for minor differences immediately adjacent to the chromophore that result from the K66M substitution.

As expected, the folds of zFP538 and DsRed are very similar (Figure 3). The polypeptide backbone of zFP538 comprises 231 residues, 6 residues longer than DsRed, with insertions in loop regions connecting the β strands. Superposition of α carbons results in rms deviation of 0.9 Å for 210 equivalent positions with DsRed. Consistent with greater sequence divergence (23% identity) compared to GFP, the backbone superposition leads to rms deviation of 1.35 Å for 190 equivalent positions, with large differences in surface loop configurations. Within the zFP538 tetramer, as compared to DsRed, there are rotations and translations of

Table 1: Crystallographic Statistics for Wild-Type and K66M zFP538[a]

data collection	wild type	K66M
space group	$P3_121$	$P6_222$
cell *a*, *b*, *c* (Å)	121.16, 121.16, 111.69	108.4, 108.4, 84.9
total observations	223 486	74 416
unique reflections	29 648	10 677
completeness[b] (%) (shell)	99.9 (99.5)	100 (100)
$I/\sigma(I)$ (shell)	10.8 (1.7)	7.8 (1.8)
R_{merge}[c] (%) (shell)	17.0 (71.0)	7.6 (40.1)
resolution (Å)	2.70	2.50
atomic model statistics		
resolution (Å)	6.0−2.7	6.0−2.5
number of reflections	23 882	9808
crystal R_{factor} (all data)	0.206	0.190
R_{work} (R_{free})	0.205 (0.255)	0.176 (0.295)
protein atoms	3529	1802
solvent atoms	79 + 2 βMC[d]	116 + 1 βMC
average *B* factor (Å^2)	45.0	40.7
average chromophore B (Å^2)	60.0 (A), 53.0 (B)	32.0
bond length deviations (Å)	0.006	0.008
bond angle deviations (deg)	1.6	1.8
B factor restraints (Å^2)	2.7	3.2

[a] Some refinement and model adjustments were made after the atomic models were deposited in the Protein Data Bank. Those depositions will be updated. [b] Completeness is the ratio of the number of observed $I > 0$ divided by the theoretically possible number of intensities. Shell refers to the highest of 10 resolution shells. [c] $R_{merge} = \sum|I_{hkl} - \langle I\rangle|/\sum\langle I\rangle$, where $\langle I\rangle$ is the average of the individual measurements of I_{hkl}. [d] β-mercaptoethanol covalently attached to a cysteine residue.

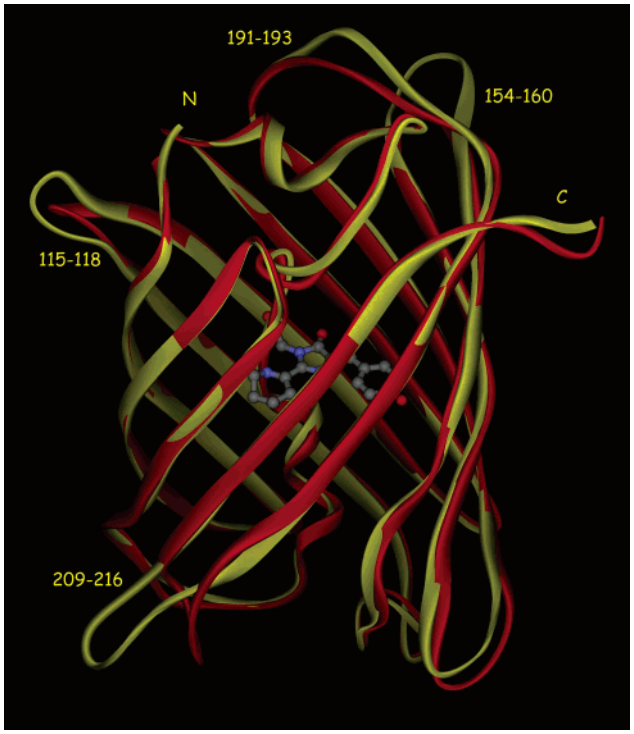

FIGURE 3: Schematic ribbon drawing of backbone superposition of DsRed (red) and wild-type zFP538 (yellow). Loops with divergent sequences are labeled with the sequence numbering of zFP538. The wild-type zFP538 chromophore is represented as a ball-and-stick model. Cys 149 (indicated) forms an intermolecular disulfide bridge within the tetramer, as described in the text.

individual subunits by 10−12° combined with translations of 1−2 Å. There are also small but significant differences in the tetrameric arrangement in the K66M and wild-type crystals. This can clearly be attributed to the oxidative formation of two intermolecular disulfide linkages per tetramer in the wild-type crystals. In each subunit, Cys 149 pairs with a symmetry counterpart across the A−C or B−D interface (chain identifiers as assigned in DsRed) (*18*). As a consequence, subunits C and D rotate in concert by about 4° relative to their arrangement in the reduced K66M tetramer. The tetramer interface characteristics are discussed in more detail and summarized in parts a and b of Supplementary Table 2 in the Supporting Information.

Chromophore and Environment. Although the diffraction is of medium resolution, the electron density maps were of high enough quality to allow straightforward interpretation of the chromophore and its environment. The electron density maps have a very similar appearance for each of the two independent subunits of the wild-type crystal. Each view leads to the conclusion that in wild-type zFP538, Lys 66 has cyclized to form a second heterocyclic ring. The approximate plane of this ring is nearly parallel with that of the rest of the chromophore (no planarity or aromatic restraints were imposed on the third ring during refinement), consistent with conjugation of the proposed C−N heterocyclic double bond with the rest of the chromophore. Furthermore, the backbone is cleaved between residues 65 and 66, resulting in a presumptive carboxamide terminal group at residue 65. The electron density maps suggest that the new terminus forms hydrogen bonds with the remnant of Lys 66 and the carbonyl oxygen of the remnant of Gly 68 (Figures 2 and 4). In contrast, the chromophore of the K66M variant is indistinguishable from that of GFP, and the continuity of the backbone preceding the chromophore is clear (Figure 2). The 65−66 peptide bond of K66M is a normal trans peptide bond, unlike the situation for DsRed where it is cis, but substantially distorted from ideal cis peptide geometry by conjugation with the rest of the chromophore (*18*, *19*).

The zFP538 chromophore environment includes a number of buried charges that form a network of salt-bridge and hydrogen-bond interactions (Figures 4 and 5), as previously observed in DsRed (*18*, *19*). DsRed and zFP538 have a similar number of positive and negative charges in the vicinity of the chromophore, including a positively charged group (residue 70) placed near the methylene, bridging the

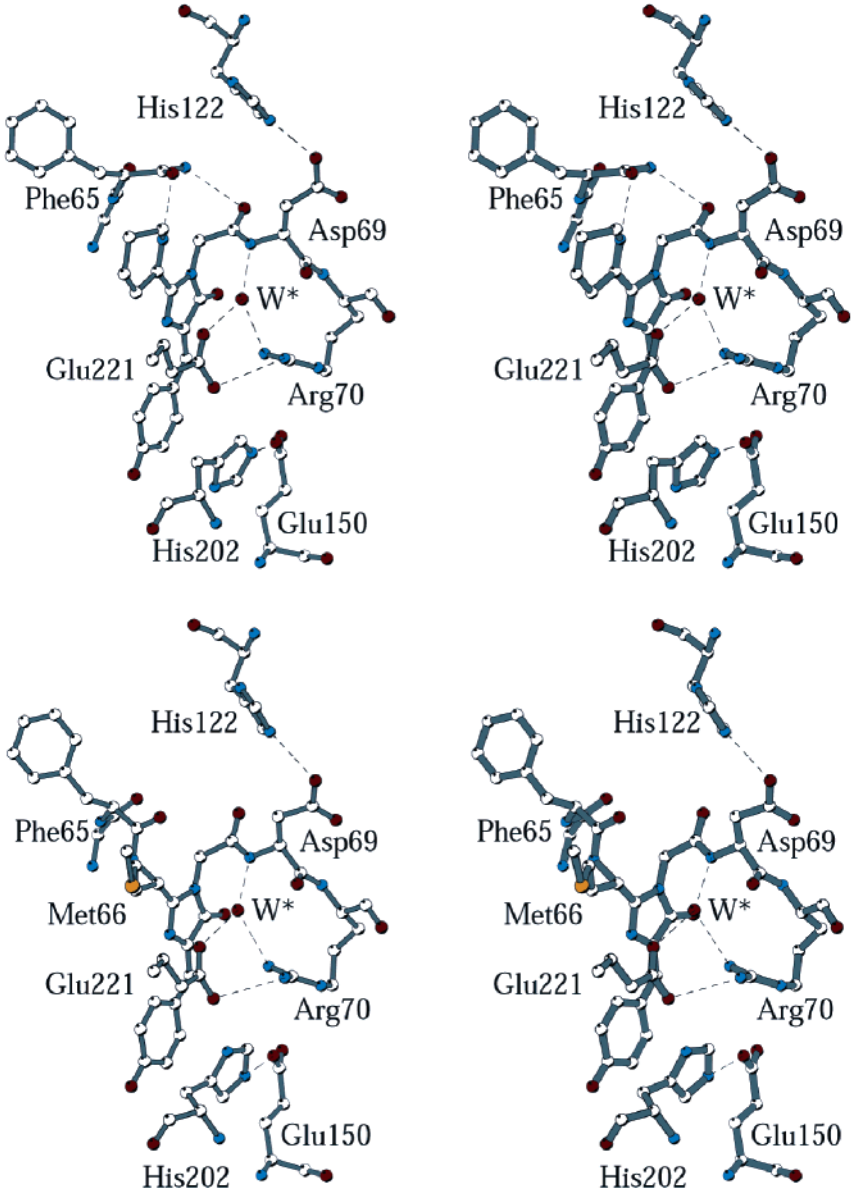

FIGURE 4: Stereoview of the ball-and-stick model of the chromophore environment in wild-type (top) and K66M (bottom) zFP538. Carbon, white; nitrogen, blue; oxygen, red; and sulfur, yellow. Dashed lines indicate hydrogen bonds or salt bridges. W* is a conserved water molecule, found in all fluorescent proteins, that may be a product of chromophore formation.

phenolate and the imidazolinone moieties (Figure 5). In zFP538, the network includes His 202, Glu 221, Arg 70, a conserved water molecule, and Glu 150, in an approximately planar configuration against one side of the chromophore. The opposite face of the chromophore packs against a hydrophobic surface. A solvent molecule (assumed to be water and labeled W* in Figures 4 and 5), coordinated by conserved Glu 221, is found centered upon the imidazolinone ring. A solvent molecule is found at this position in all fluorescent protein structures, as well as in histidine ammonia lyase (*34*), suggesting that it is a product of the ring-formation reaction.

Interestingly, the imidazole ring of His202 is π-stacked against the chromophore phenol moiety (Figure 4), reminiscent of the engineered yellow-fluorescent protein (YFP) (*35*). In YFP, a similar stacking interaction with the introduced Tyr 203 results in an emission shift from 508 to 527 nm (*36*). In zFP538, however, the interaction with His 202 is unaltered in the green-emitting K66M mutant and therefore cannot be held responsible for the yellow emission observed for wild-type zFP538. The imidazole nitrogens of His 202 are within hydrogen-bonding distance to glutamic acids Glu 221 and Glu 150, implying that the imidazole is cationic. This presumed charge is consistent with the anionic state of the chromophore and helps explain the observed low pK_a values of the chromophore in wild-type zFP538 (4.79 ± 0.04) and K66M (4.52 ± 0.03, data not shown). The substitution of methionine for lysine does not have a large effect on the dissociation constant of the chromophore, suggesting that in the wild type, Lys 66 (or its derivative) is uncharged. In DsRed, the chromophore phenolate forms a salt bridge with Lys 163 (*18*) (equivalent to Met 167 in zFP538), which is thought to be responsible for its similarly low pK_a (*16*).

Results from MS. MS was used to verify the chromophore structure as deduced from the electron density map. The atmospheric pressure MALDI−ion trap mass spectrum of

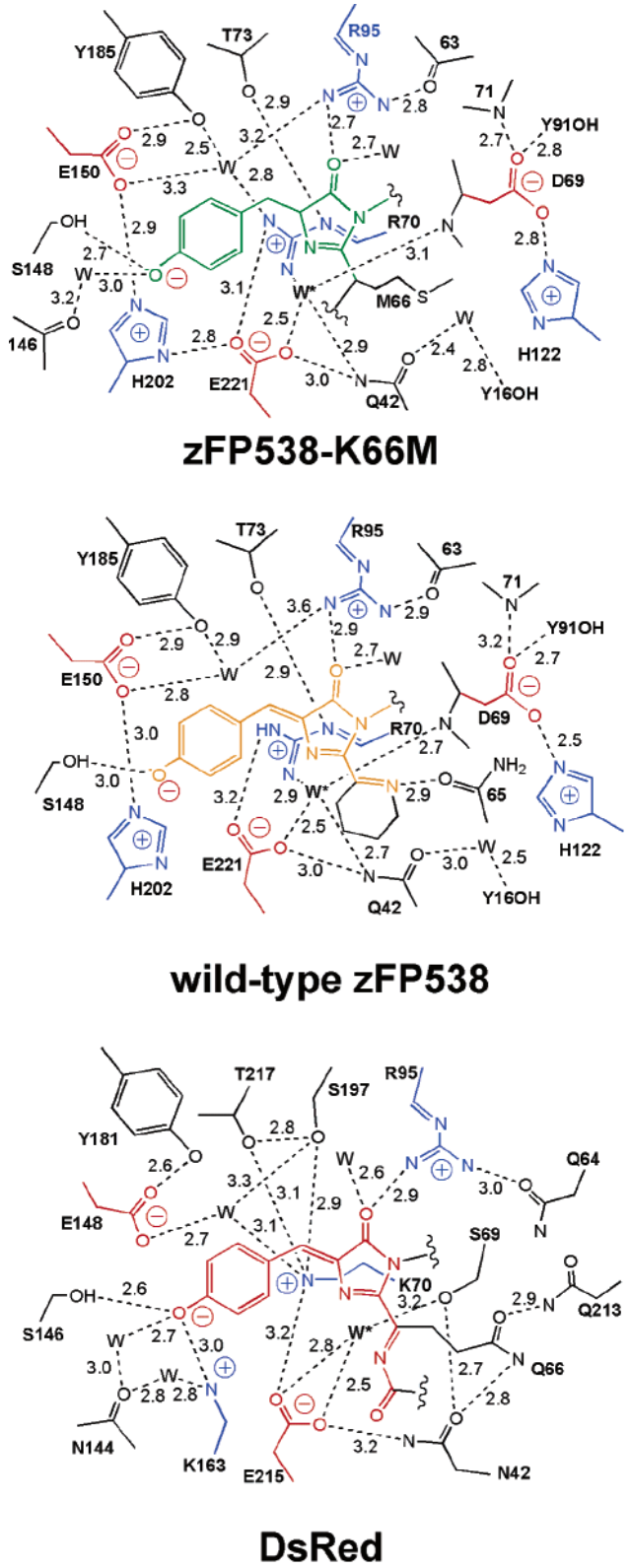

FIGURE 5: Schematic drawing comparing chromophore environments in K66M zFP538 (top), wild-type zFP538 (center), and DsRed (bottom). The dashed lines with donor−acceptor distances as indicated in angstroms denote hydrogen bonds.

the smaller tryptic chromopeptide contained four major peaks with +1 charges at 619.2, 617.2, 601.4, and 599.1 *m*/*z* (Supplementary Figure 1a in the Supporting Information) that were not present in the matrix-alone controls. These are essentially the same fragments observed by Zagranichny et al. (*24*). Fragmentation of the 599.1 *m*/*z* peak (Supplementary Figure 1b in the Supporting Information) generated peaks at 310.1, 290.3, and 175.0 *m*/*z* assigned to a $C_{17}N_3O_3H_{16}$ chromophore b1 ion, an Asp-Arg y2 ion, and an Arg y1 ion, respectively (Table 2). Fragmentation of the 310.1 *m*/*z* chromophore peak (Supplementary Figure 1c in the Supporting Information) generated peaks at 282.0, 254.2, and 227.9 *m*/*z*, consistent with the loss of CO, NCH_2CO, and the 2,3,4,5-tetrahydropyridine ring, respectively. The 599.1 *m*/*z* peak is thus consistent with a structure of the form chromophore-Asp-Arg, where the chromophore is assumed to be in the mature form found by crystallographic analysis in the intact protein (Table 2 and Supplementary Figure 3 in the Supporting Information). From additional fragmentation studies (Table 2), the 601.4 *m*/*z* peak represents a structure identical to that for the 599.1 *m*/*z* peak, except for a reduced double bond. The 619.2 and 617.2 *m*/*z* peaks represent hydrolysis products of the 601.4 and 599.1 *m*/*z* peaks, with the chromophores containing hydrolyzed imino rings with and without double-bond reduction. Hydrolysis may be acid-catalyzed in the low pH (pH ~4) matrix during the laser desorption process. These data are fully consistent with the proposed chromopeptide structure shown in Figure 1b. Interestingly, Zagranichny et al. (*24*) identified the tricyclic species in their preparations but considered it to be an artifact.

A Green Intermediate in zFP538 Maturation? The maturation kinetics of wild-type zFP538 were investigated by inducing 100 mL cultures for 2 h, rapidly purifying the expressed fluorescent protein within 0.5 h, and collecting absorbance and fluorescence scans every hour thereafter. Maturation is essentially complete by 24 h (parts A and B of Figure 6). Fluorescence spectra showed a minor component with green fluorescence (λ_{em}^{max} = 506 nm), which apparently converts to the yellow-emitting species (λ_{em}^{max} = 538 nm) during a few hours. The isosbestic point at 519 nm indicates contributions from only two species. However, analysis of absorbance spectra casts doubt on whether the green species, presumed to be a GFP-like chromophore, is an actual intermediate in the reaction producing the yellow product (Figure 6B). Indeed, peak intensities at 496 nm (green form) and 528 nm (yellow form) were found to grow throughout the experiment. No decrease was observed in the amount of the green form as would be expected for the case of an intermediate compound. These data clearly indicate that the green form is a dead-end product, most likely very similar in structure to the GFP chromophore but not an intermediate form, as might be concluded from fluorescence development. Apparently, the partial conversion of green fluorescence into yellow during zFP538 maturation is explained by efficient fluorescence resonance energy transfer (FRET) between green and yellow monomers within zFP538 tetramers.

Similar spectral behavior was observed by Verkhusha et al. for the maturation of DsRed and several variants (*17*). These authors suggested that the chromophore in DsRed and related proteins results from a transformation of the protonated (blue-absorbing) form of a GFP-like chromophore. During zFP538 maturation, we did not detect any intermediate forms by spectral methods. However, the chemical structure of the yellow chromophore implies the existence of GFP-like and DsRed-like intermediates that must absorb

Table 2: Principle Peaks in the Chromopeptide Mass Spectrum and Structural Interpretation[a]

m/z (observed)	*m/z* (calculated)	ion type[b]	structure/comment
599.2	599.3	parent	**1**, chromopeptide as isolated.
601.4	601.3	parent	**2**, reduced chromopeptide
617.2	617.3	parent	**3**, oxidized and hydrolyzed chromopeptide
619.2	619.3	parent	**4**, reduced and hydrolyzed chromopeptide
310.1	310.1	b1 ion	fragment (chromophore), see **1**
311.9	312.1	b1 ion	fragment (reduced chromophore), see **2**
290.3	290.1	y2 ion	Asp-Arg
282.0	282.1	fragment	loss of CO from chromophore
254.2	254.1	fragment	loss of NCH_2CO from chromophore
227.9	228.1	fragment	loss of C_5H_8N ring from chromophore
175.0	175.1	peptide	Arg

[a] See Supplementary Figure 1 in the Supporting Information for representative mass spectra and Supplementary Figure 2 in the Supporting Information for a structural interpretation of compounds **1**−**4**. The hydrolysis of the chromopeptide accounting for peaks 3 and 4 and corresponding fragments is assumed to have taken place in the acidified matrix (pH ∼4) during laser desorption. [b] For y and b ions, see ref *41*.

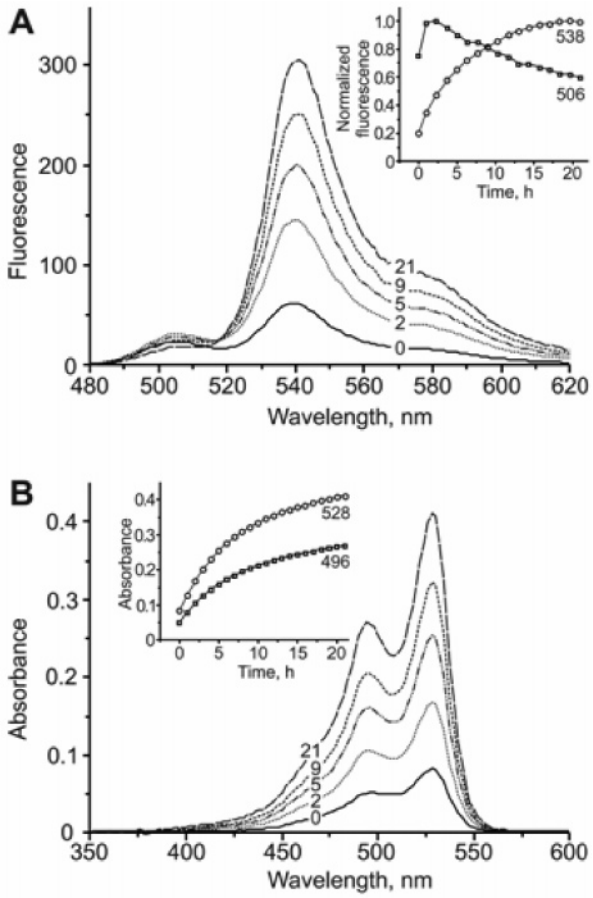

FIGURE 6: Maturation kinetics of wild-type zFP538. (A) Fluorescence changes in the course of zFP538 maturation. Emission spectra were measured using excitation at 450 nm at consecutive stages of protein maturation (0, 2, 5, 9, and 21 h after protein purification). Inset shows the time course for fluorescence development at 506 (□) and 538 (○) nm. Each dataset was normalized per its maximal value. (B) Absorption spectra for zFP538 at different stages of its maturation (0, 2, 5, 9, and 21 h after protein purification). Inset shows the time course of development of absorption peaks at 496 (□) and 528 (○) nm.

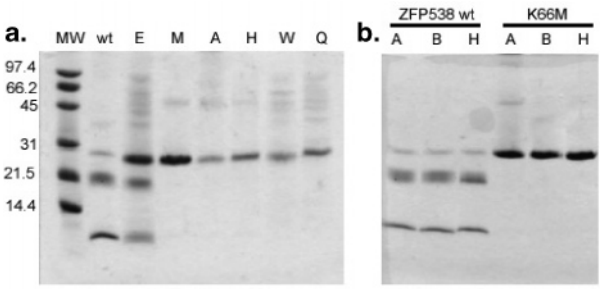

FIGURE 7: (a) SDS−PAGE analysis of wild-type and variant forms of zFP538 under denaturing conditions (samples were boiled for 1 min). The labels above the individual lanes are MW (standards), wt (wild type), or indicate by the single-letter code the substitution for lysine at position 66. (b) Comparison of different denaturation protocols used in SDS−PAGE analysis of chain cleavage in wild-type and K66M zFP538. Samples were either boiled for 1 min (H), acid-denatured (A), or base-denatured (B) as described in the Materials and Methods.

visible light. If the rate of formation of the intermediates is slower than rate of their transformation into subsequent species, then the intermediates will not accumulate to an extent permitting their detection.

Mutagenesis of Position 66 and Polypeptide Backbone Cleavage. When wild-type zFP538 is subjected to SDS−PAGE analysis, three bands are observed. A faint band corresponds to the intact monomer of M_r ∼28K, while two more intense bands correspond to fragments of M_r ∼10K and ∼18K (parts a and b of Figure 7). The band corresponding to the intact monomer probably corresponds to protein in which chromophore formation is incomplete and represents less than 10% of the total material. The electron density map of wild-type zFP538 shows no evidence for contamination by immature species, but contamination of up to 10% would probably not be detected. A similar gel pattern has been observed for DsRed with boiled samples, which is attributed to the hydrolysis of the reactive acylimine linkage adjacent to the chromophore (*15*). However, unlike DsRed, in zFP538, the chain break is observed for material denatured under acidic or basic conditions as well (lanes A and B of Figure 7b). Furthermore, the relative band intensities are independent of the boiling time (in the range of 0.5−24 min, data not shown). We conclude, in agreement with the appearance of the electron density map and the proposal of Zagranichny et al. (*24*), that within fully mature, folded zFP538, the polypeptide backbone is cleaved at the 65−66 position.

On the basis of limited mutagenesis studies, Gurskaya et al. (*23*) reported that Lys 66 is essential for the formation of the yellow emission at 538 nm. To verify the importance of lysine at position 66, we constructed, expressed, and purified proteins with all 19 possible substitutions. Most mutant proteins expressed well and produced green fluorescence with emission spectra essentially indistinguishable from that of GFP. Green mutants included the substitutions A, C, F, G,

H, L, M, N, S, T, P, Q, and V. The substitutions I, R, W, and Y resulted in proteins that were essentially nonfluorescent. All of the mutant proteins except for K66E run as a single band of approximate M_r = 28K on denaturing gels (Figure 7a), suggesting that the autocatalytic chain cleavage is linked to the final maturation step. We tested whether the substitution K66H could lead to UV-induced green → red photoconversion, as recently described for the fluorescent protein "Kaede" (*37*), but purified samples of K66H showed no evidence for photoconversion under intense UV illumination.

Acidic mutations at position 66 provide important and potentially very interesting exceptions. The substitutions K66E and K66D each yielded proteins with spectroscopic evidence for a mixture of at least two different chromophores. K66E runs as three distinct bands on SDS−PAGE (Figure 7a), consistent with a fraction of molecules suffering a chain break near the 65−66 position, but the chain in K66D appears to be intact. K66E has excitation maxima at 493 and 550 nm, with intense green (λ_{em}^{max} = 504 nm) and weak red (λ_{em}^{max} = 576 nm) emission peaks (Supplementary Figure 3 in the Supporting Information), suggesting a mixture of chromophore species. The K66D variant has emission maxima λ_{em}^{max} = 524 and 552 nm, with a broad red shoulder extending to >650 nm. One possible interpretation of these data is that the variant proteins contain a trapped acylimine intermediate similar to DsRed. In the case of K66E, this may include a species in which the Glu66 side chain has cyclized similar to the wild type, resulting in backbone cleavage.

It is interesting to note that some naturally occurring red-shifted proteins contain aspartate or glutamate in the chromophore-forming triplet. One closely related to zFP538 is the red-fluorescent protein from *Zoanthus*, zoan2RFP (*5*), which has aspartate at position 66, while glutamate at the corresponding position can be found in the blue chromoprotein hcCP from the sea anemone *Heteractis crispa* and its far-red-fluorescent mutant HcRed (*38*).

Internal Charge Network. zFP538 and DsRed are similar in that they contain an intricate network of charged groups that is not found in GFP (Figure 5). A positive charge (Lys 70) is essential for red fluorescence in DsRed, but Lys 70 may be substituted with arginine (*16*) as found in zFP538. As Figure 5 shows, with the possible exception of Glu 150 (which is involved in a salt bridge with His 202), many features of this network are not conserved between DsRed and zFP538. For example, His 202 in zFP538 is not equivalent to Lys 163 in DsRed, because they are located on opposite faces of the chromophore. Gurskaya et al. (*23*) investigated the role of Asp 69, which in zFP538 participates in an internal salt bridge with His 122 (Figures 4 and 5). Substitution with asparagine leads to incomplete maturation and mixed yellow/green emission; thus, Asp 69 is important but not essential for yellow fluorescence. The network of charged groups may be important for chromophore maturation and possibly for structural reasons, but as the structure of K66M demonstrates, the network itself is not directly responsible for yellow fluorescence.

Structural Basis for Yellow Fluorescence. We propose that the yellow emission of zFP538 is the direct result of an increase in the physical extent of the chromophore, because of the added C═N double bond in the heterocycle formed from Lys 66. We further propose that, in zFP538, the third ring is formed in a transimination reaction in which the Nϵ of Lys 66 attacks an acylimine in the polypeptide backbone. A proposed reaction scheme based on the following considerations is outlined in Figure 8.

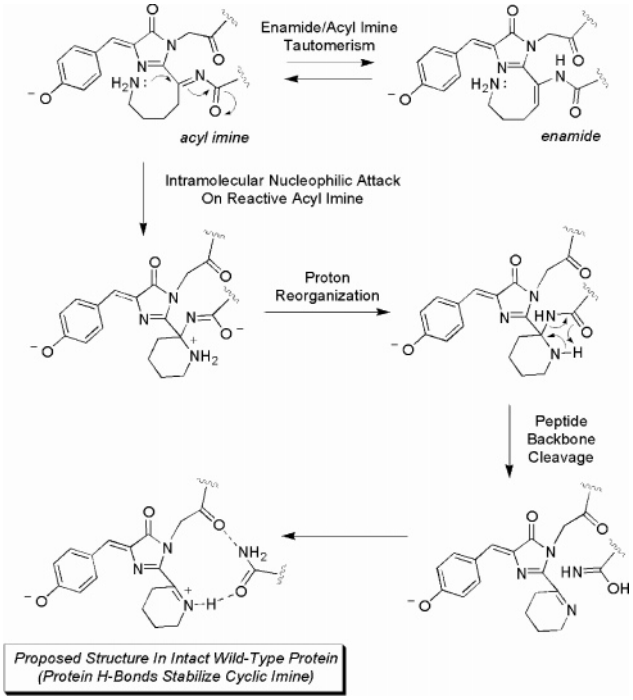

FIGURE 8: Proposed steps in the transimination reaction leading to formation of yellow-emitting chromophore in wild-type zFP538. In the final panel (bottom left), proton uptake is assumed to form the hypothetical zwitterion to account for the observed hydrogen-bond pattern of the chromophore.

The overall similarity of the active sites of DsRed and zFP538 suggests that, in both proteins, maturation should proceed to produce a green form, which is observed, and a red-emitting acylimine (*15*, *18*, *19*), which in zFP538 has not been directly observed. Although DsRed and zFP538 are rather distantly related (~42% sequence identity), a red-fluorescent protein from *Zoanthus* has been identified (*5*) with ~81% identity to zFP538; thus, the chemistry of chromophore formation should be conserved. In steps, the acylimine intermediate rearranges as shown in Figure 8, eliminating the backbone as a formal β-elimination reaction. If this reaction proceeds rapidly, the red intermediate will not accumulate to an extent permitting its detection. The cyclization reaction requires Lys 66 to be neutral, which is expected, given that the environment of Met 66 in the K66M variant is very hydrophobic. Because the lysine pK_a would be substantially depressed in this environment (*39*), the energetic cost of burying Lys 66 must be offset by the protein-folding reaction. This process could presumably provide some or all of the driving force for the acylimine intermediate → yellow product of the maturation reaction.

The formation of the acylimine, which is the endpoint of the maturation of DsRed, can be viewed as an intermediate in a reaction pathway leading to other novel chromophore species. For example, the proposed reaction scheme may be applicable to the formation of the recently observed far-red-fluorescent species with emission in the range of 615−640 nm (*38*, *40*).

ACKNOWLEDGMENT

We thank Roger Y. Tsien for helpful discussions and the staff at beam line 7-1, Stanford Synchrotron Radiation Laboratory for help with data collection.

SUPPORTING INFORMATION AVAILABLE

Two tables and three figures are available. Supplementary Table 1 shows amino acid sequence alignments of GFP, DsRed, and zFP538, while parts a and b of Supplementary Table 2 give details of side-chain interactions at the AB and AC interfaces of the zFP538 tetramer. Supplementary Figures 1 and 2 provide representative mass spectra of zFP538 chromopeptide fragments and a schematic diagram detailing the structural interpretation. Supplementary Figure 3 shows fluorescence excitation and emission spectra of the K66D and K66E mutants of zFP538. This material is available free of charge via the Internet at http://pubs.acs.org.

REFERENCES

1. Matz, M. V., Arkady, F. F., Labas, Y. A., Savitsky, A. P., Zaraisky, A. G., Markelov, M. L., and Lukyanov, S. A. (1999) Fluorescent proteins from nonbioluminescent Anthozoa species, *Nat. Biotechnol. 17*, 969−973.
2. Lukyanov, K. A., Fradkov, A. F., Gurskaya, N. G., Matz, M. V., Labas, Y. A., Savitsky, A. P., Markelov, M. L., Zaraisky, A. G., Zhao, X., Fang, Y., Tan, W., and Lukyanov, S. A. (2000) Natural animal coloration can be determined by a nonfluorescent green fluorescent protein homolog, *J. Biol. Chem. 275*, 25879−25882.
3. Dove, S., Takabayashi, M., and Hoegh-Guldberg, O. (1995) Isolation and characterization of the pink and blue pigments of Pocilloporid and Acroporid corals, *Biol. Bull. 189*, 288−297.
4. Dove, S. G., Hoegh-Guldberg, O., and Ranganathan, S. (2001) Major colour patterns of reef-building corals are due to a family of GFP-like proteins, *Coral Reefs 19*, 197−204.
5. Labas, Y. A., Gurskaya, N. G., Yanushevich, Y. G., Fradkov, A. F., Lukyanov, K. A., Lukyanov, S. A., and Matz, M. V. (2001) Diversity and evolution of the green fluorescent protein family, *Proc. Natl. Acad. Sci. U.S.A. 99*, 4256−4261.
6. Remington, S. J. (2002) Negotiating the speed bumps to fluorescence, *Nat. Biotechnol. 20*, 28−29.
7. Verkhusha, V. V., and Lukyanov, K. A. (2004) The molecular properties and applications of Anthozoa fluorescent proteins and chromoproteins, *Nat. Biotechnol. 22*, 289−196.
8. Bulina, M. E., Chudakov, D. M., Mudrik, N. N., and Lukyanov, K. A. (2002) Interconversion of Anthozoa GFP-like fluorescent and nonfluorescent proteins by mutagenesis, *BMC Biochemistry 3*.
9. Chudakov, D. M., Belousov, V. V., Zaraisky, A. G., Novoselov, V. V., Staroverov, D. B., Zorov, D. B., Lukyanov, S., and Lukyanov, K. A. (2003) Kindling fluorescent proteins for precise *in vivo* photolabeling, *Nat. Biotechnol. 21*, 191−194.
10. Chudakov, D. M., Foefanov, A. V., Mudrik, N. N., Lukyanov, S., and Lukyanov, K. A. (2003) Chromophore environment provides clue to "kindling fluorescent protein" riddle, *J. Biol. Chem. 278*, 7215−7219.
11. Campbell, R. E., Tour, O., Palmer, A. E., Steinbach, P. A., Baird, G. S., Zacharias, D. A., and Tsien, R. Y. (2002) A monomeric red fluorescent protein, *Proc. Natl. Acad. Sci. U.S.A. 99*, 7877−7882.
12. Barondeau, D. P., Putnam, C. D., Kassmann, C. J., Tainer, J. A., and Getzoff, E. D. (2003) Mechanism and energetics of green fluorescent protein chromophore synthesis revealed by trapped intermediate structures, *Proc. Natl. Acad. Sci. U.S.A. 100*, 12111−12116.
13. Rosenow, M. A., Huffman, H. A., Phail, M. E., and Wachter, R. M. (2004) The crystal structure of the Y66L variant of green fluorescent protein supports a cyclization−oxidation−dehydration mechanism for chromophore maturation, *Biochemistry 43*, 4464−4472.
14. Terskikh, A., Fradkov, A. F., Ermakova, G., Zaraisky, A. G., Tan, P., Kajava, A. V., Zhao, X., Ding, L., Lukyanov, S. A., Matz, M. V., Kim, S., Weissman, I., and Siebert, P. (2000) "Fluorescent timer": Protein that changes color with time, *Science 290*, 1478−1479.
15. Gross, L. A., Baird, G. S., Hoffman, R. C., Baldridge, K. K., and Tsien, R. Y. (2000) The structure of the chromophore within DsRed, a red fluorescent protein from coral, *Proc. Natl. Acad. Sci. U.S.A. 87*, 11990−11995.
16. Baird, G. S., Zacharias, D. A., and Tsien, R. Y. (2000) Biochemistry, mutagenesis and oligomerization of DsRed, a red fluorescent protein from coral, *Proc. Natl. Acad. Sci. U.S.A. 97*, 11984−11989.
17. Verkhusha, V. V., Chudakov, D. M., Gurskaya, N. G., Lukyanov, S., and Lukyanov, K. A. (2004) Common pathway for the red chromophore formation in fluorescent proteins and chromoproteins, *Chem. Biol. 11*, 845−854.
18. Yarbrough, D., Wachter, R. M., Kallio, K., Matz, M. V., and Remington, S. J. (2001) Refined crystal structure of DsRed, a red fluorescent protein from coral, at 2.0 Å resolution, *Proc. Natl. Acad. Sci. U.S.A. 98*, 462−467.
19. Wall, M. A., Socolich, M., and Ranganathan, R. (2000) The structural basis for red fluorescence in the tetrameric GFP homolog DsRed, *Nat. Struct. Biol. 7*, 1133−1138.
20. Petersen, J., Wilmann, P. G., Beddoe, T., Oakley, A. J., Devenish, R. J., Prescott, M., and Rossjohn, J. (2003) The 2.0 Å crystal structure of eqFP611, a far-red fluorescent protein from the sea anemone Entacmaea quadricolor, *J. Biol. Chem. 278*, 44626−44631.
21. Prescott, M., Ling, M., Beddoe, T., Oakley, A. J., Hoegh-Guldberg, O., Devenish, R. J., and Rossjohn, J. (2003) The 2.2 Å crystal structure of a pocilloporin pigment reveals a nonplanar chromophore conformation, *Structure 11*, 275−284.
22. Martynov, V. L., Maksimov, B. I., Matynova, N. Y., Pakhomov, A. A., Gurskaya, N. G., and Lukyanov, S. A. (2003) A purple-blue chromoprotein from *Goniopora tenuidens* belongs to the DsRed subfamily of GFP-like proteins, *J. Biol. Chem. 278*, 46288−46292.
23. Gurskaya, N. G., Savitsky, A. P., Yanushevich, Y. G., Lukyanov, S. A., and Lukyanov, K. A. (2001) Color transitions in coral's fluorescent proteins by site-directed mutagenesis, *BMC Biochemistry 2*.
24. Zagranichny, V. E., Rudenko, N. V., Gorokhovatsky, A. Y., Zakharov, M. V., Shenkarev, Z. O., Balashova, T. A., and Arseniev, A. S. (2004) zFP538, a yellow fluorescent protein from coral, belongs to the DsRed subfamily of GFP-like proteins but possesses the unexpected site of fragmentation, *Biochemistry 43*, 4764−4772.
25. Leslie, A. G. W. (1996) in *Crystallographic Computing* (Moras, D., Podjarny, A. D., and Thierry, J. C., Eds.) pp 50−61, Oxford University Press, Oxford, U.K.
26. Evans, P. R. (1993) Data reduction, in *Data Collection and Processing, Proceedings of the CCP4 Study Weekend* (Sawyer, L. et al., Eds.) pp 114−122, Daresbury Laboratory, Daresbury, U.K.
27. Otwinowski, Z., and Minor, W. (1997) Processing of X-ray diffraction data collected in oscillation mode, *Methods Enzymol. 276*, 307−326.
28. Kissinger, C. R., Gehlhaar, D. K., and Fogel, D. B. (1999) Rapid automated molecular replacement by evolutionary search, *Acta Crystallogr., Sect. D 55*, 484−491.
29. Tronrud, D. E., Ten Eyck, L. F., and Matthews, B. W. (1987) An efficient general-purpose least-squares refinement program for macromolecular structures, *Acta Crystallogr., Sect. A 43*, 489−503.
30. Jones, T. A., Zou, J.-Y., Cowan, S. W., and Kjeldgaard, M. (1991) Improved methods for building protein models in electron density maps and the location of errors in these models, *Acta Crystallogr., Sect. A 47*, 110−119.
31. Brunger, A. T., Adams, P. D., Clore, G. M., DeLano, W. L., Gros, P., Grosse-Kunstleve, R. W., Jiang, J.-S., Kuszewski, J., Nilges, M., Pannu, N. S., Read, R. J., Rice, L. M., Simonson, T., and Warren, G. L. (1998) Crystallography and NMR Systems: A new software suite for macromolecular structure determination, *Acta Crystallogr., Sect. D 54*, 905−921.
32. Brunger, A. T. (1997) Free *R* value: Cross-validation in crystallography, *Methods Enzymol. 277*, 366−396.
33. Laskowski, R. A., MacArthur, M. W., Moss, D. S., and Thornton, J. M. (1993) PROCHECK: A program to check the stereochemical quality of protein structures, *J. Appl. Crystallogr. 26*, 283−291.

34. Schwede, T. F., Retey, J., and Schulz, G. E. (1999) Crystal structure of histidine ammonia-lyase revealing a novel polypeptide modification as the catalytic electrophile, *Biochemistry 38*, 5355−5361.
35. Ormo, M., Cubitt, A. B., Kallio, K., Gross, L. A., Tsien, R. Y., and Remington, S. J. (1996) Crystal structure of the *Aequorea victoria* green fluorescent protein, *Science 273*, 1392−1395.
36. Wachter, R. M., Elsliger, M. A., Kallio, K., Hanson, G. T., and Remington, S. J. (1998) Structural basis of spectral shifts in the yellow-emission variants of green fluorescent protein, *Structure 6*, 1267−1277.
37. Ando, R., Hama, H., Yamamoto-Hino, M., Mizuno, H., and Miyawaki, A. (2002) An optical marker based on the UV-induced green-to-red photoconversion of a fluorescent protein, *Proc. Natl. Acad. Sci. U.S.A. 99*, 12651−12656.
38. Gurskaya, N. G., Fradkov, A. F., Terskikh, A., Matz, M. V., Labas, Y. A., Martynov, V. I., Yanushevich, Y. G., Lukyanov, K. A., and Lukyanov, S. A. (2001) GFP-like chromoproteins as a source of far-red fluorescent proteins, *FEBS Lett. 507*, 16−20.
39. Dao-pin, S., Anderson, D. E., Baase, W. A., Dahlquist, F. W., and Matthews, B. W. (1991) The structural and thermodynamic consequences of burying a charged residue within the hydrophobic core of T4 lysozyme, *Biochemistry 30*, 11521−11529.
40. Fradkov, A. F., Chen, Y., Ding, L., Barsova, E. V., Matz, M. V., and Lukyanov, S. A. (2000) Novel fluorescent protein from Discosoma coral and its mutants possesses a unique far-red fluorescence, *FEBS Lett. 479*, 127−130.

BI048383R